European Geothermal Congress 2022
Berlin, Germany | 17-21 October 2022
www.europeangeothermalcongress.eu

Integration of ground-source heat pumps in combined district heating and cooling networks: A holistic modeling framework

Marwan Abugabbara[1], Maria Alberdi-Pagola[2], Saqib Javed[1], Søren Erbs Poulsen[3]

[1] Department of Building and Environmental Technology, Division of Building Services, Lund University, 221 00 Lund, Sweden

[2] Centrum Pæle A/S and cp test A/S, Grønlandsvej 96, 7100 Vejle, Denmark

[3] Research Center for Built Environment, Energy, Water and Climate, VIA University College, 8700 Horsens, Denmark

marwan.abugabbara@hvac.lth.se

Keywords: Ground-source heat pumps, Geothermal bore field, district heating and cooling, Modelica.

ABSTRACT

The integration of heat pumps in low-enthalpy district heating and cooling networks can increase the efficiency and flexibility of the network. In such systems, heat pumps are installed both locally and centrally to serve different functions. In the former case, decentralized heat pumps at each building adjust the low-network temperature to the desired supply temperature. In the latter case, a central and relatively large-scale heat pump functions as a heat source or a heat sink to the ground. The main benefits of such technology are the reduction of the network operating temperature, the ability to supply simultaneous heating and cooling by operating the heat pumps in either heating or cooling mode, and the increased potential to integrate low-enthalpy shallow geothermal energy for heat generation and heat storage. One technical challenge in accelerating the implementation of this technology is the complexity of modeling the entire district network including all its components. A holistic modeling framework based on the equation-based objected-oriented Modelica language is presented in this paper. We first describe the three component models included in the framework, namely, the building substations, the distribution pipes, and the shallow geothermal bore field. Then, an example of a campus area consisting of eight buildings with varying heating and cooling demands is presented to apply the modeling framework and to demonstrate the expected mechanism by which such systems may operate. Simulation results indicate that high system performance can be attained when 1) the building supply temperature is controlled using demand-based temperature control curves, 2) the network operates at low-temperature close to the ground temperature, and 3) the bore field is balanced with sufficient heat injection to the ground. For future investigations, the modeling framework should be extended to cover the economic and the environmental impact of such systems due to the importance of these aspects in the planning of energy systems.

1. INTRODUCTION

District heating and cooling (DHC) networks play a key role in the transition to future urban energy-efficient systems. Heat pumps connected to district networks are a particular technology that can increase both the efficiency and the flexibility of the network. Recent technologies of DHC networks operate at low water temperatures in the range of 5-40 °C. In general, the water temperature is not suited for the direct supply to connected buildings. Therefore, local water-source heat pumps are installed at each building and an additional benefit for supplying simultaneous heating and cooling can be realized depending on the building demand type. Because of the low water temperature in the district network, the potential for integrating low-enthalpy renewable energy sources to function as a heat source and/or heat sink becomes larger. Ground-source heat pumps (GSHP) coupled with combined DHC networks is a promising solution that incorporates the benefits of shallow geothermal energy and low-temperature DHC networks into one integrated system.

Sweden has the highest installation rate per capita of GSHP with 650 000 units installed in 2020 (IEA, 2021). The Nordic country has also a large market share of district heating networks which provide about 60 % of the total heat delivered to all Swedish buildings (Werner, 2017). The main energy sources for producing heat in the Swedish district heating system are biomass and municipal solid waste. The integration of GSHP in DHC networks would therefore cover a significant share of the Swedish heating market using a renewable source of energy. Lately, a few studies have shed light on the role of utilizing shallow geothermal energy in DHC networks to supply heating and cooling to entire communities (Tester et al., 2021; Zeh et al., 2021). A shallow geothermal bore field provides a relatively stable and high fluid temperature during winter, which yields better system performance compared to other

energy sources, e.g., rivers, lakes, or ambient air. Similarly, excess heat in summer, that would otherwise be wasted, is injected into the bore field and benefits in reducing the required size of the bore field. Moreover, the excess heat is stored for later use and decreases the bore field depletion which results from the continuous heat extraction from the ground over long periods.

Modeling and simulation of GSHP integrated into DHC networks is a wide topic that encompasses several research areas. On the one hand, heating and cooling demands for an individual building are obtained at the design stage from a whole-building energy simulation program such as EnergyPlus (Crawley et al., 2001), TRNSYS (Klein et al., 1976), and IDA-ICE (EQUA, 2021). For urban-scale analysis of heating and cooling demands with sustainable energy planning, the use of other tools like EBSILON®Proffessional (Steag-System Technologies, 2021) and EnergyPlan (Sustainable Energy Planning Research group at Aalborg University, 2022) becomes important. On the other hand, tools dedicated to sizing ground heat exchangers and evaluating the fluid temperature are needed. Common tools used in this field are Earth Energy Designer known as EED (Hellström & Sanner, 1994) and GLHEPRO (Spitler, 2000).

Modelica is a free open-source new generation tool recommended by the International Energy Agency for the modeling and simulation of building and community energy systems (Wetter & Van Treeck, 2017). It enables modeling complex systems by decomposing them into smaller component models that are connected through connection lines. These lines interface the model variables with the other connected models, and hence, there are no strict inputs and outputs to the model. Instead, the variables are computed by efficient solvers as long as the boundary conditions at the connection ports are sufficient to solve the system of equations. Variables are standardized at the connection ports depending on the model domain. For instance, standardized variables in the hydraulic domain are mass flow and pressure. While in the thermal domain these are the heat flow rate and temperature.

This paper aims to present a framework for modeling GSHP integrated into DHC networks. Section 2 describes the modeling framework including the three main component models found in such systems. Section 3 demonstrates an example for the modeling and simulation of a geothermal district heating and cooling system using demand profiles from eight buildings located in south Sweden. The main conclusions are finally outlined in Section 4.

2. MODELING FRAMEWORK

An overview of the framework for modeling GSHP integrated into a DHC network using Modelica is shown in Figure 1. The framework consists of three main parts that cover the building substations, the district pipe network, and the geothermal bore field. Figure 1 shows typical inputs and outputs to each of these parts. In the following subsections, a description of the models used in these three parts is provided separately.

2.1 Building substation model

Different technical installations may exist in the building substation (BSS) depending on the building demand type. A building substation with both heating and cooling demands typically includes a heat pump, a mechanical chiller, circulation pumps, and a heat exchanger that is used for direct cooling when the district network temperature is cold enough to be used for direct supply. Each of these installations can be modeled by reusing existing component models from the Modelica *Buildings* library (Wetter et al., 2014).

Heat pumps are modeled by reusing the existing component model found in `Buildings.Fluid.HeatPumps.Carnot_TCon`. The model takes varying heat demands and supply temperatures as inputs. Although it is possible to model entire buildings in Modelica, this approach is not recommended as it results in thousands

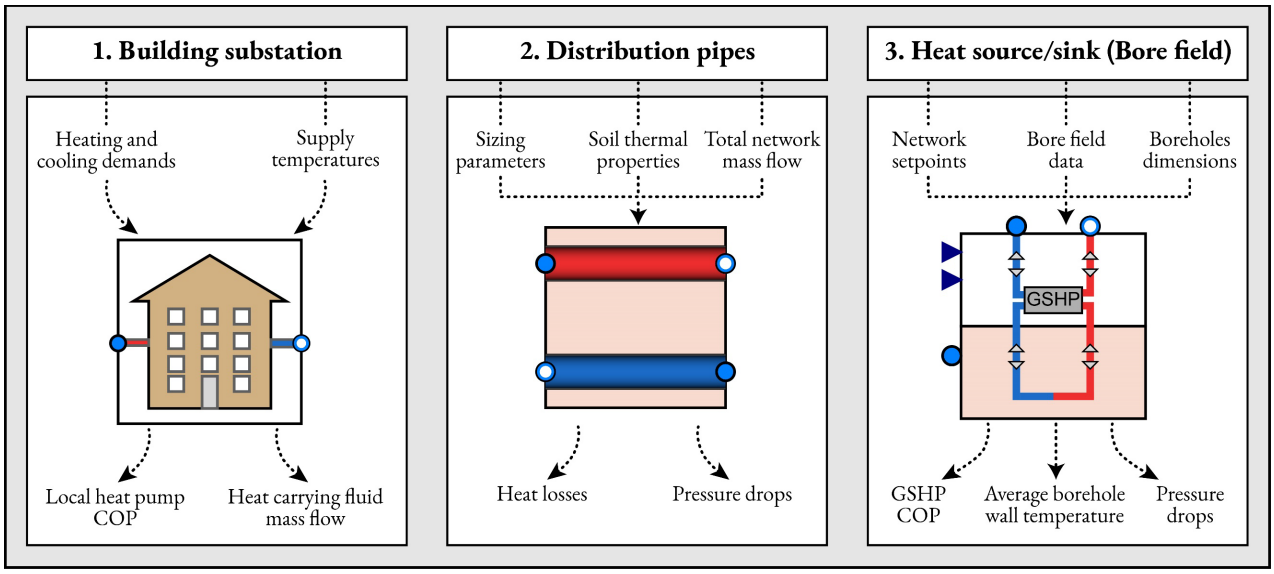

Figure 1: A Modelica framework for modeling GSHP integrated into a DHC network with examples of typical inputs and outputs in each component model.

of differential equations to be solved. Instead, heating demands and supply temperatures can be obtained from either actual measurements or simulation results from another program depending on which data is available. When the heating demand of a building at a particular point in time is known, the mass flow entering the heat pump condenser is determined as:

$$\dot{m}_{con} = \frac{\dot{Q}_h}{\Delta T_{con} \cdot c_{p,water}} \quad [1]$$

where $\dot{Q}_h$ is the heating demand, ΔT_{con} is the temperature difference between the condenser outlet and inlet, and $c_{p,water}$ is the specific heat capacity of water.

The heat pump coefficient of performance (COP) is scaled according to a prescribed Carnot efficiency as:

$$COP_{HP} = \eta_{Carnot} \cdot \frac{T_{con}}{T_{con} - T_{eva}} \quad [2]$$

where η_{Carnot} is the Carnot efficiency, T_{con} and T_{eva} are the condenser and evaporator temperatures.

The supply temperature is controlled using a demand-based temperature control that aims to increase the potential for energy savings (Zhou et al., 2014). This type of controller is not influenced by the outdoor temperature as is the case in typical outdoor temperature-compensated control curves. Rather, the quantity of thermal demand is proportional to a lower and an upper boundaries of supply temperatures. As Figure 2 shows, the lower and upper boundaries of the supply temperature are proportional to the 25th and 75th percentile of the heating and cooling demands. The reader is reminded that cooling demands are denoted by a negative sign and are therefore placed on the left side of the cartesian plane.

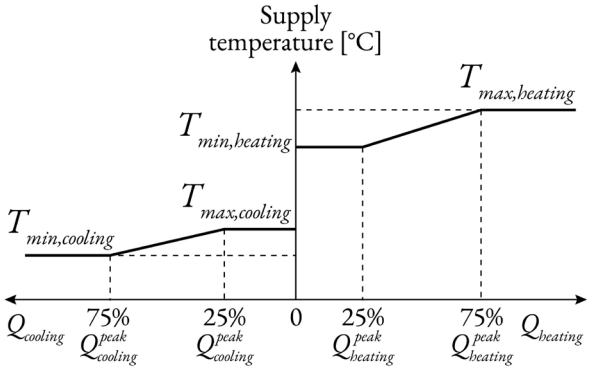

Figure 2: Demand-based temperature control curves.

Mechanical chillers are modeled in a similar way to heat pumps, except that the COP calculation shown in Equation 2 is modified by replacing the condenser temperature in the nominator with the evaporator temperature.

As for circulation pumps, the component model `Buildings.Fluid.Movers.FlowControlled_m_flow` is used to calculate the variable pump power as:

$$P_{pump} = \frac{\dot{V} \cdot \Delta p}{\eta_h \cdot \eta_m} \quad [3]$$

where $\dot{V}$ is the volume flow, Δp is the pump pressure rise, η_h is the pump hydraulic efficiency, and η_m is the motor hydraulic efficiency.

The last component in the BSS is the direct cooling heat exchanger which is modeled using an instance of `Buildings.Fluid.HeatExchangers.DryCoilEffectivenessNTU` where its heat transfer rate is equivalent to:

$$\dot{Q} = \varepsilon \cdot \dot{m} \cdot c_{p,water} \cdot \left(T_{pri,in} - T_{sec,in}\right) \quad [4]$$

where ε is the heat exchanger effectiveness that is computed dynamically based on the number of transfer units, the ratio between minimum to maximum flow rate, and the flow regime; $\dot{m}$ is the maximum mass flow circulating the heat exchanger; $T_{pri,in}$ and $T_{sec,in}$ are respectively the primary and secondary loops inlet temperatures.

2.2 Distribution pipe model

The model for the distribution network presented in this study is constructed based on a two-pipe topology with a parallel connection to buildings and bidirectional mass flow. The pipes are uninsulated and are made of high-density polyethylene. The model is divided into two parts that take into account both hydraulic and thermal aspects of the distribution pipe. The hydraulic part is generally expressed by the relationship between the mass flow and the pressure drop as:

$$\dot{m} = k \cdot \sqrt{\Delta p} \quad [5]$$

where k is a fixed flow resistance that is derived from nominal design parameters. The nominal pressure loss due to friction at the wall of the distribution pipe is computed according to the flow regime as described in detail in the Modelica implementation provided in reference (Modelica, 2020).

The second part of the distribution pipe model is related to the heat losses (or heat gains) in the pipe. As Figure 3 shows, the model accounts for the interaction between the pipe and the surrounding soil (referred to as the symmetrical problem) as well as the interaction between the two pipes (referred to as the anti-symmetrical problem). The calculations of heat losses are based

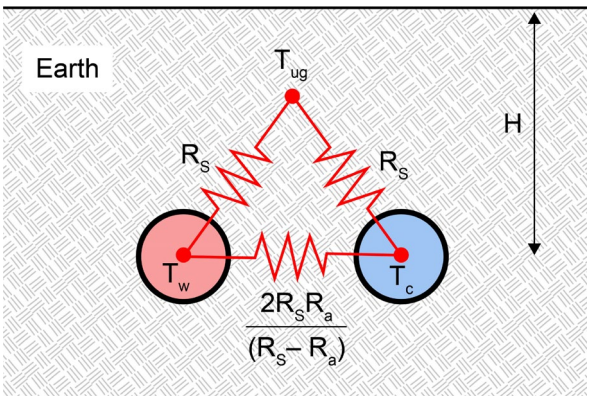

Figure 3: Representation of thermal resistances for pipe heat loss calculations.

on steady-state conditions using the multipole method described by Wallentén (1991) and detailed in Standard SS-EN 13941-1 (Svenska institutet för standarder, 2021).

The derivation of the thermal resistance for the symmetrical problem R_s is expressed as:

$$R_s = \frac{1}{2 \cdot \pi \cdot \lambda_{soil}} \cdot \left[ln\left(\frac{4 \cdot H_o}{D}\right) + \beta + ln\left(\sqrt{1 + \left(\frac{2 \cdot H_o}{C}\right)^2}\right)\right] \quad [6]$$

where λ_{soil} is the soil thermal conductivity, H_o is a corrected pipe burial depth which considers the surface resistance, D is the pipe outer diameter, C is the distance between the center of the two pipes, and β is a dimensionless resistance parameter that is determined as:

$$\beta = \frac{\lambda_{soil}}{\lambda_{pipe}} \cdot ln\left(\frac{D}{d}\right) \quad [7]$$

where λ_{pipe} is the pipe thermal conductivity, and d is the pipe inner diameter. Similarly, the thermal resistance for the anti-symmetrical problem R_s is expressed as:

$$R_s = \frac{1}{2 \cdot \pi \cdot \lambda_{soil}} \cdot \left[ln\left(\frac{4 \cdot H_o}{D}\right) + \beta - ln\left(\sqrt{1 + \left(\frac{2 \cdot H_o}{C}\right)^2}\right)\right] \quad [8]$$

Once the undisturbed ground temperature T_{ug} is prescribed and the fluid temperature in the warm and cold pipes are evaluated during simulations, heat losses (or heat gains) in the distribution pipes are determined accordingly.

2.3 Bore field model

The last part of the modeling framework is related to the geothermal bore field. The earliest implementation of a bore field model in Modelica was carried out by Picard and Helsen (2014). The model was later extended and detailed in the work of Laferrière et al. (2020). The model is capable of simulating any arbitrary configuration of boreholes while taking into account the short- and long-term responses. The short-term response evolves at time scales from minutes to hours and is related to the transient thermal effects of the fluid through the borehole and the transient heat conduction through the filling material. The long-term response, on the other hand, takes place at time scales from weeks to months where the interactions between the boreholes in the bore field become significant. The bore field model assumes that the boreholes are connected in parallel and that all of the boreholes have uniform dimensions. An overview of the structure of the bore field model is presented in Figure 4 which constitutes the following two parts: 1) borehole model, and 2) ground model.

2.2.1 Borehole model

For a single borehole like the one illustrated in Figure 4, the borehole model describes the heat transfer from the heat carrying fluid to the borehole wall. The borehole is vertically discretized into segments of equal length in order to account for the vertical variations of the fluid temperature. The conductive heat transfer between the borehole segments is not considered, while an identical borehole wall temperature is applied to each segment. Inside each segment, the so-called delta-circuit of thermal resistances represents the heat transfer between the fluid and the borehole. To include the capacitance of the fluid and the filling material, the delta-circuit developed by Bauer et al. (2011) is used in the model. The model is currently available for only single U-tube and double U-tube (parallel or series connection) configurations. The illustration in Figure 4 is depicted for the single U-tube configuration and the calculations of the thermal resistances based on Bauer et al. (2011) are reproduced below to gain more clarity. The presented notations are adopted from the Modelica implementation.

The thermal resistance between the fluid and the grout is expressed as:

$$R_{fg} = \frac{1}{Nu \cdot \pi \cdot \lambda_f} + \frac{ln\left(\frac{r_{Tub}}{r_{Tub,in}}\right)}{2 \cdot \pi \cdot \lambda_p} + x \cdot R_g \quad [9]$$

where Nu is the fluid Nusselt number, λ_f and λ_p are the fluid and pipe thermal conductivity, r_{Tub} and $r_{Tub,in}$ are the tube outer and inner radius, x is the position of the center of mass of the grout, and R_g is the thermal resistance from the outer pipe wall to the borehole wall. x and R_g are calculated as:

$$x = \frac{ln\left(\frac{\sqrt{{r_b}^2 + 2 \cdot {r_{Tub}}^2}}{2 \cdot r_{Tub}}\right)}{ln\left(\frac{r_b}{2 \cdot r_{Tub}}\right)} \quad [10]$$

$$R_g = 2 \cdot R_b - \frac{1}{Nu \cdot \pi \cdot \lambda_f} - \frac{ln\left(\frac{r_{Tub}}{r_{Tub,in}}\right)}{2 \cdot \pi \cdot \lambda_p} \quad [11]$$

where r_b is the borehole radius, R_b is the fluid to ground thermal resistance which is derived using the multipole method described by Claesson & Hellström (2011) and implemented in Modelica for internal evaluation.

The thermal resistance between the two grouting zones can be calculated as:

$$R_{gg} = \frac{2 \cdot R_{gb}\left(R_{ar} - 2 \cdot x \cdot R_g\right)}{2 \cdot R_{gb} - R_{ar} + 2 \cdot x \cdot R_g} \quad [12]$$

where R_{gb} is the thermal resistance between the grout and the borehole wall, and R_{ar} is the thermal resistance between the outer wall of the two pipes. R_{gb} and R_{ar} are determined as:

$$R_{gb} = (1 - x)R_g \quad [13]$$

$$R_{ar} = R_a - 2\left(\frac{1}{Nu \cdot \pi \cdot \lambda_f} + \frac{ln\left(\frac{r_{Tub}}{r_{Tub,in}}\right)}{2 \cdot \pi \cdot \lambda_p}\right) \quad [14]$$

where R_a is the total resistance when the heat flux at the borehole boundaries is zero, which is also defined by Claesson & Hellström (2011).

Finally, the capacity of the grout and the fluid are expressed as:

$$C_g = \rho_g \cdot \frac{\pi}{4}\left(2 \cdot {r_b}^2 - 2{r_{Tub}}^2\right)c_{p,g} \quad [15]$$

$$C_f = \rho_f \cdot c_{p,f} \cdot \frac{\pi}{4} \cdot 2{r_{Tub,in}}^2 \quad [16]$$

where ρ_g and ρ_f are the grout and fluid density, and $c_{p,g}$ and $c_{p,f}$ are the grout and fluid specific heat capacity.

2.2.2 Ground model

The second part of the bore field model is intended for the description of the heat transfer in the ground, as shown in Figure 4. Heat extraction or injection from the ground depends on the heating and cooling demands of the buildings connected to the district network. It is customary to present building heating and cooling demands using annual hourly time resolution, while higher resolutions up to 15 minutes are becoming more common to investigate peak demands. When performing multi-year simulations of the bore field, using hourly resolution becomes computationally taxing. Therefore, the ground model uses the load aggregation method proposed by Claesson & Javed (2012) to reduce the required computational time. Since Modelica runs in the continuous-time domain, Laferrière et al. (2020) have presented adjustments to the load aggregation method of Claesson & Javed (2012) to allow simulations using variable time steps. In such adjustments, the bore field temperature response, also known as the *g-function*, gives the relation between the variation of the

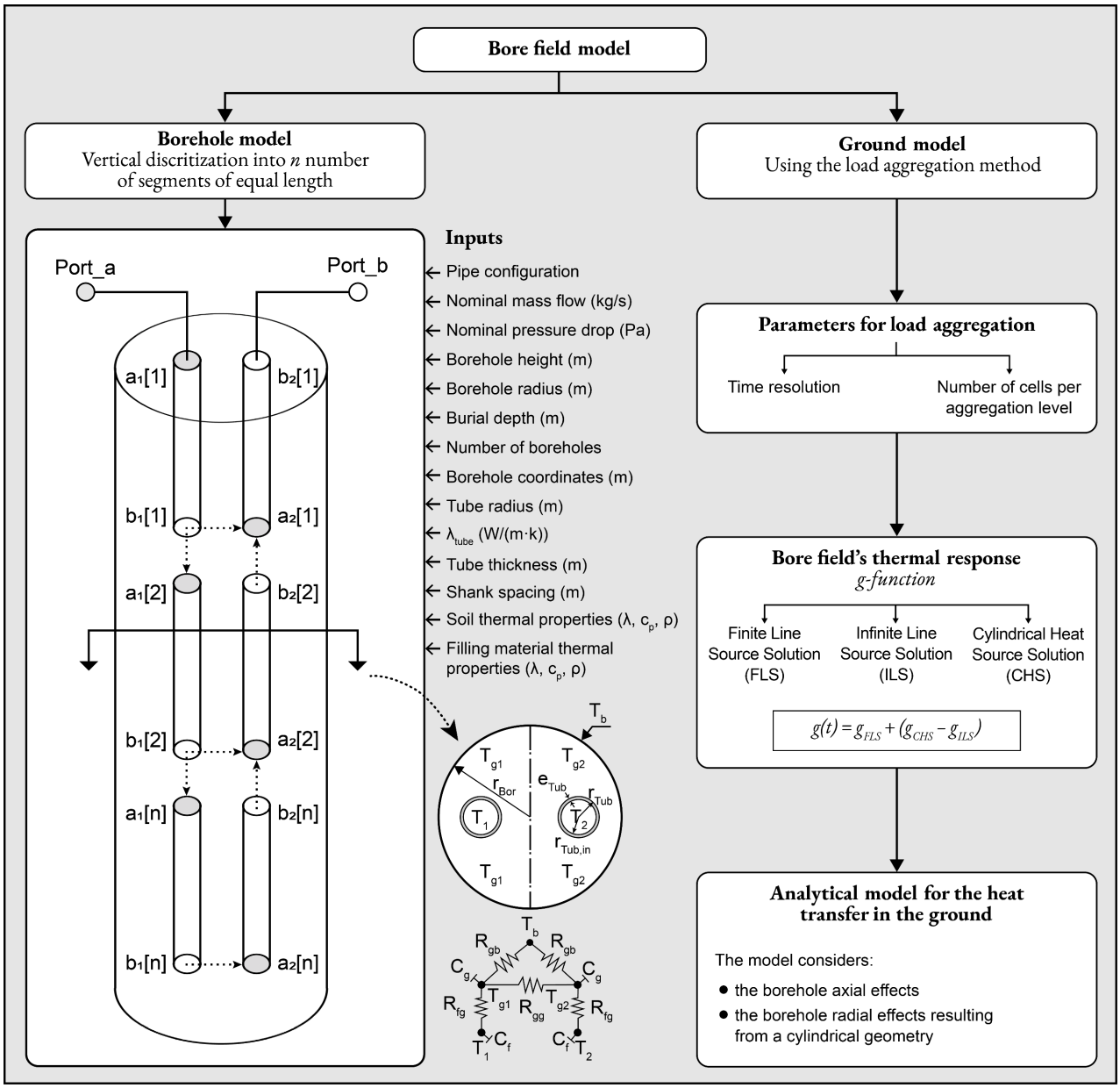

Figure 4: Bore field model structure. The borehole model is shown for a single U-tube configuration where heat extraction from the ground is indicated by a flow direction from port_a to port_b. The delta-circuit of thermal resistances is adopted from Bauer et al. (2011).

borehole wall temperature at a certain point in time and the heat extraction and injection rates at all preceding times. The concept of the g-function was originally introduced by Eskilson (1987) and its Modelica evaluation follows the method described by Cimmino & Bernier (2014) and later refined by Cimmino (2018). In such a method, the g-function is evaluated for each unique bore field design data as a combination of the finite line source (FLS) solution, the cylindrical heat source (CHS) solution, and the infinite line source (ILS) solution. A correction of the g-function that considers the cylindrical geometry is considered as proposed by Li et al. (2014) and expressed as:

$$g(t) = g_{FLS} + (g_{CHS} - g_{ILS}) \quad [17]$$

Finally, a convolution integral between the heat flux at the borehole wall and the bore field's thermal response factor is used to model the heat transfer in the ground analytically as:

$$\Delta T_b(t) = \int_0^t Q(\tau) \cdot \frac{dT_{step}(t-\tau)}{d\tau} d\tau \quad [18]$$

where ΔT_b is the difference in the borehole wall temperature, Q is the heat flux at the borehole wall, and dT_{step} is the ground temperature response.

3. EXAMPLE

This section presents an example of a ground-source heat pump integrated into a district network consisting of eight buildings with simultaneously and hourly varying heating and cooling demands which is located in south Sweden. Let Figure 5 show the Modelica diagram view of the district system including its three main component models that are previously presented in the modeling framework shown in Figure 1. On the lower left side of the figure, the GSHP model encapsulates the geothermal bore field while the heat pump cooling and heating setpoints are defined externally to maintain the network temperature within limits defined by the user. All boreholes are for a single U-tube configuration and are filled with grout. Values of the parameters used in the GSHP model are provided in Table 1.

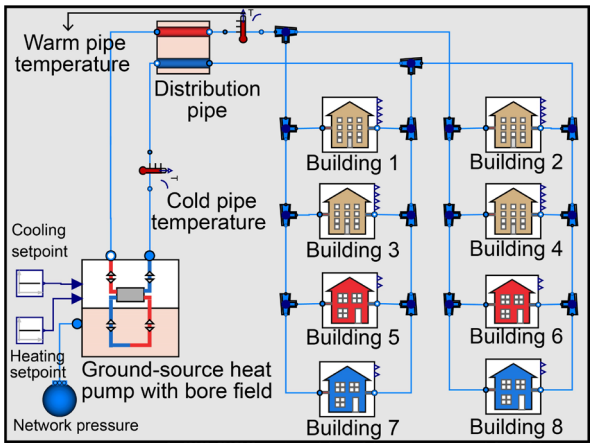

Figure 5: Modelica diagram view of a geothermally driven district network with eight connected buildings.

The second component model in the district system is denoted by the distribution pipe model. Here, pressure drops and heat losses across the longitudinal direction are computed as discussed earlier in Section 2.2. To simplify the model, all distribution pipes, including connection pipes, are lumped into one component with parameter values shown in Table 2. The connection between the main distribution pipe and each building is realized by a flow junction that has no pressure drops.

Table 1: Parameters for the GSHP and the bore field models.

Parameter	Value	Unit
GSHP heating setpoint	18	°C
GSHP cooling setpoint	20	°C
GSHP pressure drops over district loop	6000	Pa
GSHP ΔT over bore field loop	4	K
GSHP Carnot effectiveness	0.5	-
Number of boreholes	200	-
Borehole height	300	m
Borehole burial depth	5	m
Borehole radius	0.057	m
Bore field nominal pressure drops	35000	Pa
Number of borehole segments	10	-
U-tube pipe outer diameter	40	mm
U-tube pipe thickness	2.3	mm
U-tube pipe thermal conductivity	0.4	W/m·K
Shank spacing	35	mm
Grout thermal conductivity	2	W/m·K
Grout volumetric heat capacity ($\rho_g \cdot c_{p,g}$)	1.95e6	J/m^3·K
Ground thermal conductivity	3	W/m·K
Ground thermal diffusivity	1.3e-6	m/s^2
Undisturbed ground temperature	10.3	°C
Load aggregation time resolution	3600	s
Number of cells per aggregation level	5	-

Table 2: Parameters for the distribution pipe model.

Parameter	Value	Unit
Pipe total length	1000	m
Pipe outer diameter	250	mm
Pipe wall thickness	14.8	mm
Pipe surface roughness	2.5e-5	m
Pipe thermal conductivity	0.17	W/m·K
Soil thermal conductivity	1.6	W/m·K
Burial depth	0.8	m
Spacing between the outer wall of the pipes	0.2	m
Fluid velocity at nominal mass flow	1.0	m/s

The last component model represents the building substation, which draws water from either the warm or cold district pipe based on the building demand type. Building icons denoted in yellow indicate building substations with both heating and cooling demands. Table 3 shows the parameters in the BSS and their values. The heat pumps in each BSS have infinite capacity, implying that the entire BSS demand over the simulation period is provided solely by the heat pump.

Figure 6 shows different simulation results of the district system. A greater understanding of the network demand profiles can be attained from Figure 6(a) and Figure 6(b) which present the cumulative sum of annual hourly power demand and energy for all eight build-

Table 3: Parameters for the building substation model.

Parameter	Value	Unit
Heating maximum supply temperature	45	°C
Heating minimum supply temperature	35	°C
Cooling maximum supply temperature	12	°C
Cooling minimum supply temperature	7	°C
Heat pump ΔT over building loop	4	K
Heat pump ΔT over district loop	4	K
Heat pump Carnot effectiveness	0.5	-
Heat pump nominal pressure drops over condenser and evaporator	30000	Pa

ings. It can be seen that the network requires varying and simultaneous heating and cooling demands throughout the year. The heating peak power demand occurs first in February and later in November with a value of about 4 MW. Almost throughout the year, there is a constant cooling power demand of 0.5 MW, where the peak cooling power occurs in July with about 6 MW. From an energy perspective, the network has annual energy demands for heating and cooling of 8 and 5 GWh, respectively. These values suggest that the presented demand profile may increase the potential for exchanging energy flows between connected buildings while also balancing the bore field by injecting the summer excess heat into the ground after a continuous heat extraction in winter.

The amount of heat extracted and injected from/into the ground is illustrated in Figure 6(c). By contrasting Figure 6(a) with Figure 6(c), one can notice that heat extraction from the ground takes place when the network heating demand is dominant. On the contrary, network cooling demands dominate in winter and therefore excess heat is injected into the ground. Simulation results of the corresponding mass flow circulating through the bore field are shown in Figure 6(d). The amount of mass flow in the bore field varies based on the extracted or injected heat and according to the GSHP design temperature difference over the bore field loop. This, in turn, influences the bore field entering and leaving temperatures as shown in Figure 6(e). Here, the starting temperature of the fluid leaving the bore field is equivalent to the undisturbed ground temperature. In winter months when heat is extracted from the ground, the heat carrying fluid enters the bore field after exchanging heat with the evaporator of the GSHP. In spring and autumn, heat extraction and heat injection occur repetitively in short periods, causing rapid changes in the bore field entering temperature. The entering temperature to the bore field becomes higher as heat injection into the ground becomes more salient in summer.

The temperature of the fluid in the distribution pipe is presented in Figure 6(f) according to the sensors' location shown previously in Figure 5. In a heating mode during winter, the heat carrying fluid leaving the bore field enters the evaporator of the GSHP. At the condenser side, the GSHP maintains the temperature of the warm district pipe such that it does not fall below a heating setpoint of 18 °C. The fluctuations in the simulated fluid temperature in the distribution pipes are attributed to the heat losses to the surrounding ground and the heat exchange between the two pipes. The opposite of the previous process takes place in summer months when the GSHP operates in cooling mode. The evaporator of the GSHP maintains the temperature of the cold pipe at a cooling setpoint of 20 °C. Rapid changes in the fluid temperature in the distribution pipes occur when network heating and cooling demands are almost

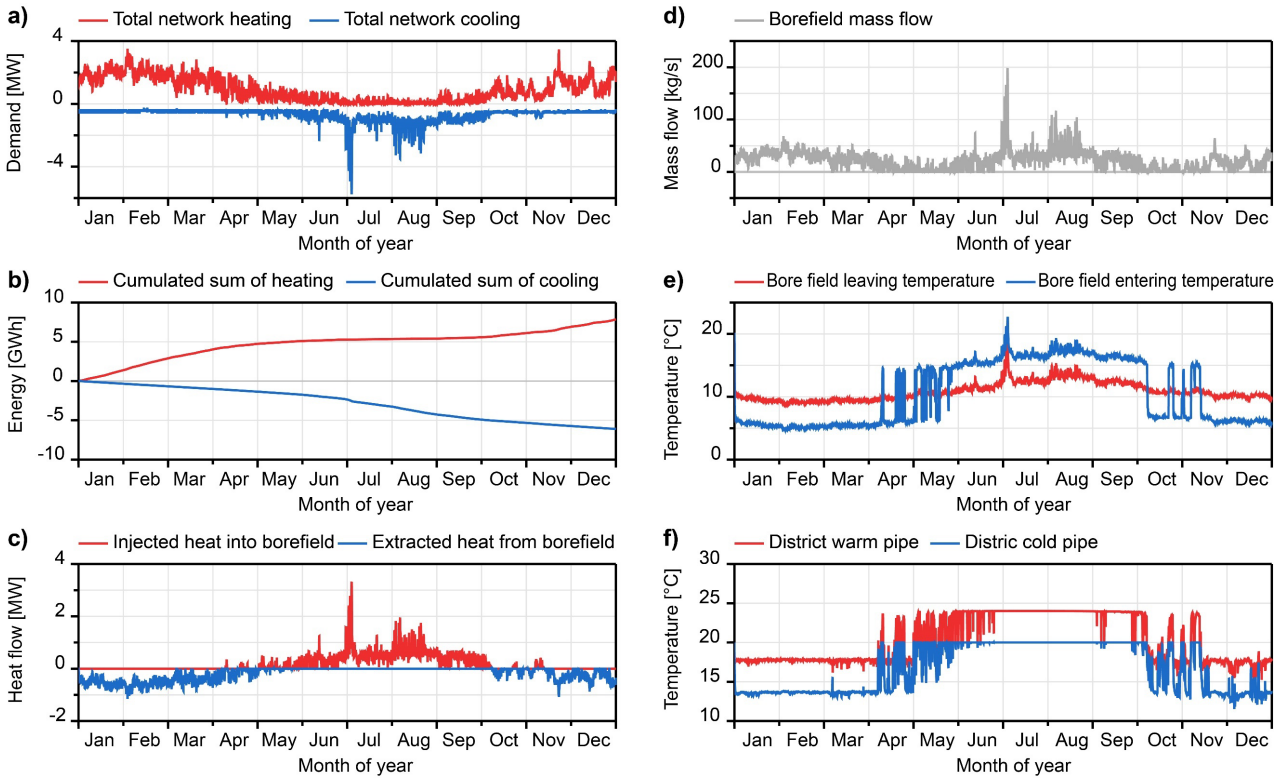

Figure 6: Simulation results for different component models and output variables.

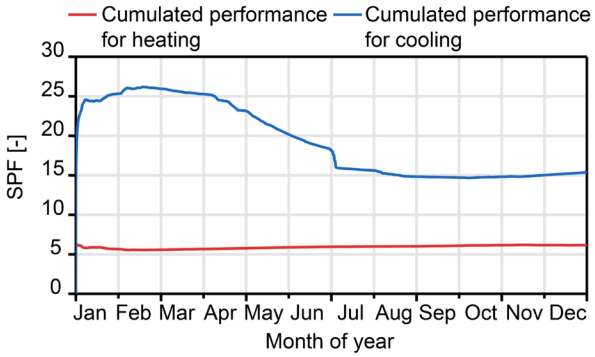

Figure 7: Annual cumulated Seasonal Performance Factor of the entire district system.

similar in quantity to each other, as is case during spring and autumn. This leads to quick changes in the type of dominant demand in the network and, hence, quick changes in the operating mode of the GSHP.

As for the system performance, Figure 7 shows the cumulated seasonal performance factor (SPF) for both heating and cooling. The boundaries for calculating the system SPF include the electric power use in all circulation pumps and compressors installed in the GSHP and the eight building substations. A superior heating and cooling SPF of 6 and 15 was possible to achieve compared to traditional individual heating and cooling systems that have lower performance. The simulated system performance is based on the abovementioned network operating conditions and the given parameter values. Two main reasons are related to the obtained high performance. The first of which is the use of the demand-based temperature control curves in all building substations. Such a controller has a significant improvement on the performance of the local heat pumps when compared against using conventional outdoor temperature-compensated control curves that usually force the heat pump to operate at higher supply temperatures for longer periods of time. The second reason is related to the low temperature difference between the fluid in the bore field and the network setpoints. This, ultimately, causes the GSHP to operate at low temperature lifts and therefore improves its performance.

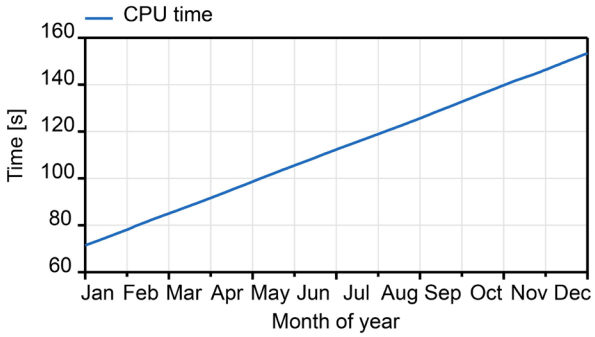

Figure 8: Computational time for annual simulation of the district system.

The final presented result in this example shows the computational time required to perform an annual simulation of the entire district system including eight connected buildings and a geothermal bore field. A desktop computer with 12 physical cores and a maximum speed of 3.5 GHz and 32 GB of RAM was used to run the simulation. As Figure 8 shows, the simulation of the entire district system took about two and a half minutes to perform. About half of the time (71 seconds) is related to the initialization time where the bore field g-function is evaluated. The g-function is stored locally in the model subdirectory and is recalled when another simulation using the same bore field design data is performed. Thus, the revaluation of the g-function is not needed, and the time required to perform the new simulation can be reduced by half.

4. CONCLUSIONS

A modeling framework to evaluate and assist further research and development on the integration of ground-source heat pumps in combined district heating and cooling networks was presented in this paper. The framework is based on the Modelica language which supports the free use and edit of existing robust component models for building and community energy systems. The paper briefly described the main component models that are used when simulating a geothermal bore field connected to a district heating and cooling network. An example was presented to show the modeling of a geothermal district heating and cooling network consisting of eight buildings with varying heating and cooling demands and a bore field of 200 boreholes. Simulation results indicate promising potentials for a wider implementation of low-temperature district networks integrated with shallow geothermal energy. Moreover, the ability to conduct model-based research on similar systems is increased since the annual simulation of the presented example took about one minute to perform.

FUNDING

This work was financially supported by the European Regional Development Fund, program Interreg Öresund-Kattegat-Skagerrak, project COOLGEOHEAT: Shallow geothermal energy – the green and effective heating and cooling grids of the future, under grant number [NYPS 20293146].

REFERENCES

Bauer, D., Heidemann, W., Müller-Steinhagen, H., & Diersch, H.-J. G. (2011). Thermal resistance and capacity models for borehole heat exchangers. *International Journal of Energy Research*, *35*(4), 312–320. https://doi.org/https://doi.org/10.1002/er.1689

Cimmino, M. (2018). Fast calculation of the g-functions of geothermal borehole fields using similarities in the evaluation of the finite line source solution. *Journal of Building Performance Simulation*, *11*(6), 655–668. https://doi.org/10.1080/19401493.2017.1423390

Cimmino, M., & Bernier, M. (2014). A semi-analytical method to generate g-functions for geothermal bore fields. *International Journal of Heat and Mass Transfer*, *70*, 641–650.

https://doi.org/10.1016/J.IJHEATMASSTRANSFER.2013.11.037

Claesson, J., & Hellström, G. (2011). Multipole method to calculate borehole thermal resistances in a borehole heat exchanger. *HVAC\&R Research*, *17*(6), 895–911. https://doi.org/10.1080/10789669.2011.609927

Claesson, J., & Javed, S. (2012). A Load-Aggregation Method to Calculate Extraction Temperatures of Borehole Heat Exchangers. *ASHRAE Transactions*, *118*, 530–539.

Crawley, D. B., Lawrie, L. K., Winkelmann, F. C., Buhl, W. F., Huang, Y. J., Pedersen, C. O., … Glazer, J. (2001). EnergyPlus: Creating a new-generation building energy simulation program. *Energy and Buildings*. https://doi.org/10.1016/S0378-7788(00)00114-6

EQUA. (2021). IDA Indoor Climate and Energy. Stockholm. Retrieved from https://www.equa.se/en/ida-ice

Eskilson, P. (1987). *Thermal analysis of heat extraction boreholes*. PhD Thesis. Department of Physics, Lund University.

Hellström, G., & Sanner, B. (1994). Software for dimensioning of deep boreholes for heat extraction. *Proc. Calorstock*, *94*, 195–202.

IEA. (2021). *Heat Pumps*. Paris. Retrieved from https://www.iea.org/reports/heat-pumps

Klein, S. A., Beckman, W. A., & Duffie, J. A. (1976). TRNSYS - A TRANSIENT SIMULATION PROGRAM. *ASHRAE Transactions*.

Laferrière, A., Cimmino, M., Picard, D., & Helsen, L. (2020). Development and validation of a full-time-scale semi-analytical model for the short- and long-term simulation of vertical geothermal bore fields. *Geothermics*, *86*, 101788. https://doi.org/10.1016/J.GEOTHERMICS.2019.101788

Li, M., Li, P., Chan, V., & Lai, A. C. K. (2014). Full-scale temperature response function (G-function) for heat transfer by borehole ground heat exchangers (GHEs) from sub-hour to decades. *Applied Energy*, *136*, 197–205. https://doi.org/10.1016/J.APENERGY.2014.09.013

Modelica. (2020). WallFriction documentation. Retrieved May 18, 2022, from https://doc.modelica.org/Modelica 4.0.0/Resources/helpDymola/Modelica_Fluid_UsersGuide_ComponentDefinition.html#Modelica.Fluid.UsersGuide.ComponentDefinition.WallFriction

Picard, D., & Helsen, L. (2014). Advanced Hybrid Model for Borefield Heat Exchanger Performance Evaluation, an Implementation in Modelica. *Proceedings of the 10th International Modelica Conference, March 10-12, 2014, Lund, Sweden*, *96*, 857–866. https://doi.org/10.3384/ecp14096857

Spitler, J. D. (2000). GLHEPRO-A design tool for commercial building ground loop heat exchangers. In *Proceedings of the fourth international heat pumps in cold climates conference*.

Steag-System Technologies. (2021). EBSILON®Professional. Retrieved from https://www.steag-systemtechnologies.com/en/products/ebsilon-professional/

Sustainable Energy Planning Research group at Aalborg University. (2022). EnergyPlan: Advanced energy system analysis computer model. Retrieved from https://www.energyplan.eu/

Svenska institutet för standarder. (2021). *SS-EN 13941-1:2019 District heating pipes – Design and installation of thermal insulated bonded single and twin pipe systems for directly buried hot water networks – Part 1: Design*.

Tester, J. W., Beckers, K. F., Hawkins, A. J., & Lukawski, M. Z. (2021). The evolving role of geothermal energy for decarbonizing the United States †. *Energy Environ. Sci*, *14*, 6211. https://doi.org/10.1039/d1ee02309h

Wallentén, P. (1991). *Steady-state heat loss from insulated pipes*. PhD Thesis. Byggnadsfysik LTH, Lunds Tekniska Högskola.

Werner, S. (2017). District heating and cooling in Sweden. *Energy*, *126*, 419–429. https://doi.org/10.1016/j.energy.2017.03.052

Wetter, M., & Van Treeck, C. (2017). *New Generation Computational Tools for Building and Community Energy Systems Annex 60 Final Report*. https://doi.org/10.4103/0973-1229.86137

Wetter, M., Zuo, W., Nouidui, T. S., & Pang, X. (2014). Modelica Buildings library. *Journal of Building Performance Simulation*, *7*(4), 253–270. https://doi.org/10.1080/19401493.2013.765506

Zeh, R., Ohlsen, B., Philipp, D., Bertermann, D., Kotz, T., Jocić, N., & Stockinger, V. (2021). Large-Scale Geothermal Collector Systems for 5th Generation District Heating and Cooling Networks. *Sustainability*, *13*(11). https://doi.org/10.3390/su13116035

Zhou, P., Huang, G., & Li, Z. (2014). Demand-based temperature control of large-scale rooms aided by wireless sensor network: Energy saving potential analysis. *Energy and Buildings*, *68*(PARTA), 532–540. https://doi.org/10.1016/J.ENBUILD.2013.10.005